Nuclear Medicine and Biology 42 (2015) 643–653

Contents lists available at ScienceDirect

Nuclear Medicine and Biology

journal homepage: www.elsevier.com/locate/nucmedbio

Radiolabeling of [^{18}F]-fluoroethylnormemantine and initial in vivo evaluation of this innovative PET tracer for imaging the PCP sites of NMDA receptors☆

Anne-Sophie Salabert [a,b,e,*], Caroline Fonta [c,d], Charlotte Fontan [a,b,e], Djilali Adel [a,b], Mathieu Alonso [e], Carine Pestourie [f], Hafid Belhadj-Tahar [g], Mathieu Tafani [a,b,e], Pierre Payoux [a,b,h]

[a] Brain Imaging and Neurological Disability UMR 825, INSERM, F-31059 Toulouse, France
[b] Brain imaging and neurological disability UMR 825, University of Toulouse, UPS, CHU Purpan, Place du Dr Baylac, F-31059 Toulouse Cedex 9, France
[c] Research Center for Brain and Cognition, University of Toulouse UPS, Toulouse, France
[d] CerCo, CNRS, Toulouse, France
[e] Radiopharmacy Department, University Hospital, Toulouse, France
[f] Animal experimentation platform, UMS 006, Toulouse, France
[g] Research and Expertise Group, French Association for the Promotion of Medical Research (AFPREMED), Toulouse, France
[h] Nuclear Medicine Department, University Hospital, Toulouse, France

ARTICLE INFO

Article history:
Received 22 January 2015
Received in revised form 19 March 2015
Accepted 1 April 2015

Keywords:
Activated NMDA receptor
Innovative PET probe
preclinical
Memantine
Neuropathology
Excitatory neurotransmission

ABSTRACT

Introduction: The *N*-methyl-D-aspartate receptor (NMDAr) is an ionotropic receptor that mediates excitatory transmission. NMDAr overexcitation is thought to be involved in neurological and neuropsychiatric disorders such as Alzheimer disease and schizophrenia. We synthesized [^{18}F]-fluoroethylnormemantine ([^{18}F]-FNM), a memantine derivative that binds to phencyclidine (PCP) sites within the NMDA channel pore. These sites are primarily accessible when the channel is in the active and *open* state.

Methods: Radiosynthesis was carried out using the Raytest® SynChrom R&D fluorination module. Affinity of this new compound was determined by competition assay. We ran a kinetic study in rats and computed a time–activity curve based on a volume-of-interest analysis, using CARIMAS® software. We performed an ex vivo autoradiography, exposing frozen rat brain sections to a phosphorscreen. Adjacent sections were used to detect NMDAr by immunohistochemistry with an anti-NR1 antibody. As a control of the specificity of our compound for NMDAr, we used a rat anesthetized with ketamine. Correlation analysis was performed with ImageJ software between signal of autoradiography and immunostaining.

Results: Fluorination yield was 10.5% (end of synthesis), with a mean activity of 3145 MBq and a specific activity above 355 GBq/μmol. Affinity assessment allowed us to determine [^{19}F]-FNM IC50 at 6.1 10^{-6} M. [^{18}F]-FMN concentration gradually increased in the brain, stabilizing at 40 minutes post injection. The brain-to-blood ratio was 6, and 0.4% of the injected dose was found in the brain. Combined ex vivo autoradiography and immunohistochemical staining demonstrated colocalization of NMDAr and [^{18}F]-FNM ($r = 0.622$, $p < 0.0001$). The highest intensity was found in the cortex and cerebellum, and the lowest in white matter. A low and homogeneous signal corresponding to unspecific binding was observed when PCP sites were blocked with ketamine.

Conclusions: [^{18}F]-FNM appears to be a promising tracer for imaging NMDAr activity for undertaking preclinical studies in perspective of clinical detection of neurological or neuropsychological disorders

1. Introduction

The *N*-methyl-D-aspartate receptor (NMDAr) is an ionotropic receptor that mediates excitatory transmission in the central nervous system, controlling the opening of ion channels, and thereby permitting the prolonged influx of ions. Under physiological conditions, it is thought to play a central role in many biological functions, including neurotransmission, neuroprotection, neurodegeneration, long-term potentiation, memory and neurogenesis [1]. Conventional NMDAr requires the dual agonists glutamate and glycine for activation. Its activity is modulated by extracellular Mg^{2+}, which exerts a voltage-dependent blockade of the open ion channel [2]. Under normal conditions of synaptic transmission, NMDAr is activated for only brief periods of time. Its opening allows for the influx of Ca^{2+} and other cations. Under pathological conditions, however, overactivation of the receptor relieves the Mg^{2+} blockade and causes excessive Ca^{2+} influx into the nerve cell, triggering a variety of processes that can lead to necrosis, apoptosis, or dendritic damage. These damaging processes include Ca^{2+} overload of

☆ This is a free access article and can also be viewed on the journal's Web site (www.nucmedio.com). Complimentary access to this article is available until the next issue publishes online.

* Corresponding author at: INSERM UMR 825 Pavillon Baudot-CHU Purpan, Place du Dr Joseph Baylac, 31024 Toulouse cedex 3, France. Tel.: +33 5 62 74 61 66.
E-mail address: anne-sophie.salabert@inserm.fr (A.-S. Salabert).

http://dx.doi.org/10.1016/j.nucmedbio.2015.04.001
0969-8051/

Table 1
Characteristics of [^{18} F] radioligand for imaging PCP sites of NMDAr.

Family	Affinity [3H] TCP displacement	Lipophilicity	Molecular weight	Reference and characteristics
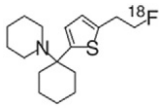 [^{18}F]FE-TCP and analogs	Kd: 38 nM	Log P: 4.83	294.5	High non-specific binding due to its high lipophilicity. [15]
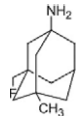 18F-FMEM	IC 50 = 6000 nM	Log P: 2.3–2.6	197.3	Good correlation with localization of NMDAr but to high uptake in WM [16–18]
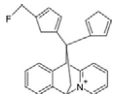 Benzoquinolizinium and analogs	IC50: 47 nM	Log P: −1.40	368.46	[22] No in vivo evaluation No test of BBB crossing
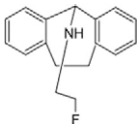 MK-801 analogs	Kd: 79 nM	Log P: 5.25	271	No specific binding in vivo [13]
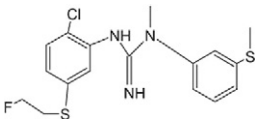 Diarylguanine analogs	Kd: 2.35 nM	Log P: 2.49	383.9	[19] Good in vivo results require further characterization with in vivo studies using activation and disease models
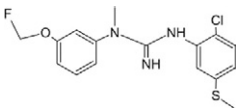	Kd: 18 nM	Log P: 3.75	354.8	High affinity and selectivity But high in vivo metabolism [21]

Affinity [represented by dissociation constant (Kd) or inhibitory concentration 50 (IC50)], lipophilicity [represented by octanol–water partition coefficient (log P)] and molecular weight. All these elements allow us to determine whether these compounds would be good brain radiotracers.

mitochondria, which results in oxygen free radical formation, caspase activation, and the release of apoptosis-inducing factor [3]. NMDArs are composed of one GluN1 (NR-1 subunit) and select combinations of GluN2 (NR-2 subunits) [4] and GluN3 (NR-3 subunits) [5]. Subcellular localization is another key factor in sensitivity to overactivation. In addition to their synaptic localization, NMDArs are found at extrasynaptic sites (more than 100 nm from the postsynaptic density [6]). Extrasynaptic NMDArs may be activated by glutamate spillover either from synapses or from the ectopic release of glutamate. As a result, extrasynaptic NMDArs may be activated in different circumstances from synaptic NMDArs. In some cases, activation of extrasynaptic NMDArs may have a negative influence on the neuron [7]. This mechanism seems to be involved in a number of neurological and neuropsychiatric disorders, including Alzheimer disease [8,9], schizophrenia, alcoholism, epilepsy and stroke [10].

We chose to develop a PCP site ligand that selectively binds to the ion channel in the open and active state. There are many noncompetitive PCP site antagonists, and several potential radioligands have already been synthesized with several different radioisotopes ([^{11}C], [^{18} F], [^{123}I]) and recently reviewed [11–13]. First came MK-801 analogs [14], ketamine [15], phencyclidine or thienyl-phencyclidine analogues [16], and memantine [17–19], because they are well known antagonists of the intrachannel site of NMDAr. However, although many compounds were tested, for many of them, binding was too nonspecific, and brain retention was poor. Another class of ligands (benzoquinolizinium) was also tested, but did not show any promising imaging characteristics because of a poor ability to penetrate the blood–brain barrier (BBB) and no specific accumulation in any brain areas [20,21]. Some other compound classes are still under investigation, such as fluoroalkyl diarylaguanidine [22]. An [^{18}F] analog of CNS5161 was recently injected in humans and has yielded promising results [23], while [^{18}F]-PK209, a new derivative of fluoroalkyl diaryguanidine, has shown interesting results in terms of affinity and selectivity in monkeys [24]. The affinity of these compounds has not yet been tested specifically for extrasynaptic receptors. In Table 1, we summarize the characteristics of members of the [^{18}F] radioligand family that have already been synthesized for imaging the PCP sites of NMDAr. (Affinity values were provided by literature data.) Many of these compounds have now been discarded.

Table 2
Pharmacological characteristics of memantine family.

Name and formula	Affinity	Lipophily	Molecular weight	References and characteristics
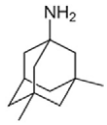 Memantine	Ki: 6.5 10^{-7} M	Log P: 3.3	179.30	Lead structure Extrasynaptic NMDAr predilection [23].
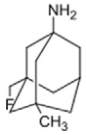 ^{18}[F]-FMEM	IC 50 = 6000 nM	Log P: 2.3–2.6	197.3	Good correlation with localization of NMDAr but too high uptake in WM[16–18]
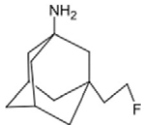 ^{18}[F]-FNM	**Ki: 3.5 10^{-6} M IC = 6000 nM**	**Log D: 1.93** (experimental)	197.3	In experiment [26] **Good correlation with localization of NMDAr.** **Low uptake in white matter: good signal on noise** **Pharmacokinetic compatible with PET imaging (40 min after injection)**

In bold, data obtained from the present study.

Memantine is an open channel blocker with a fast off-rate, and its uncompetitive nature makes it an effective blocker of chronic extrasynaptic NMDAr [25,26]. Xia et al. demonstrated that under pathological conditions, when NMDARs are overactivated and Mg^{2+} is repelled from the channels because of depolarization, memantine exhibits preferential blockade of extrasynaptic over synaptic NMDAR-mediated currents in hippocampal autapses. Wu et al. conclude in the same way in rat "substancia nigra" dopamine neuron [27]. However, another team found that memantine blocked all NMDAR populations in dopamine neurons but the degree of blockade depended on the intensity of agonist presentation at the NMDAR. This study suggests that memantine could preferentially inhibit over-active glutamatergic NMDAR signaling, but have negligible effects on low frequency synaptic signaling [28].

A derivative of memantine (^{18}[F]-FMEM) has already been synthesized [18]and tested. It has shown promising in vitro and in vivo binding in mice and monkeys [19], with good retention in the brain. However, investigations of this tracer's binding characteristics in humans have shown that its distribution does not reflect regional NMDAr concentration, owing to high nonspecific uptake in white matter [17]. We therefore chose to work on another memantine analogue, namely fluoroethylnormemantine (^{18}[F]-FNM), and to test its nonspecific binding in white matter. With its low molecular weight and its lipophilic properties, ^{18}[F]-FNM would reasonably be able to cross the BBB. We describe below the process of radiosynthesis, and the investigations of in vitro and ex vivo binding we carried out to establish the binding characteristics of ^{18}[F]-FNM (Table 2).

2. Methods

2.1. Radiochemical synthesis

2.1.1. Reagents and apparatus

A pre-conditioned Sep-Pak® Light QMA cartridge with CO_3^{2-} as counter ions and an elution reagent (600 μl with 22 mg of cryptand 222, 7 mg of potassium carbonate, 300 μl of acetonitrile, 300 μl of water for injection) were obtained from ABX Advanced Biomedical Compounds (Radeberg, Germany). A C_{18} Sep-Pak® plus cartridge was obtained from Waters (Milford, MA, USA). This cartridge was then conditioned with 5 ml of ethanol, followed by 5 ml of sterile water. Radioactivity was determined using a calibrated ion chamber (Capintec CRC-15®). Automated synthesis was carried out in the Raytest® SynChrom R&D fluorination module. HPLC (high performance liquid chromotography) for ^{18}[F]-FNM purification was carried out in the Raytest® module's built-in HPLC system featuring a semipreparative reversed-phase C_{18} column (10 × 250 mm) and a C_{18} sep pack precolumn. The semipreparative column was equipped with a UV detector (Knauer K200 micro UV detector) and a radioactivity detector (Raytest® Ramona). For quality control, HPLC analysis was carried out on a modular HPLC system with a Phenomenex® Luna® reversed-phase analytic C_{18} column (4.6 × 150 mm). The UV signal was monitored with a UV lambda max detector at 217 nm. ^{18}[F]-FNM precursor and ^{19}[F]-FNM reference standards were obtained from M2i Development (http://www.m2i-development.com).

2.1.2. Automated synthesis of ^{18}[F]-FNM

The automated radiochemical synthesis of ^{18}[F]-FNM is a two-step reaction, summarized in Fig. 1. The first reaction corresponds to the nucleophilic substitution by fluorination of 1-[*N*-(tert-butyloxy)carbamoyl]-3-(tosyl)ethyl-adamantane (1) in DMSO (dimethylsulfoxyde). The fluorinated compound tert-butyl [3-(2-fluoroethyl)tricyclo[3.3.1.13,7]dec-1-yl] carbamate (2) is hydrolyzed by hydrochloric acid at 110 °C in 3-(2-fluoroethyl)tricyclo[3.3.1.13,7]decan-1-aminium (3), and neutralized by a mixture of sodium hydroxide and trisodium citrate, to obtain ^{18}[F]-FNM: 3(2-fluoroethyl)tricyclo[3.3.1.13,7]decan-1-amine (4). Total synthesis duration is 80 minutes. Before feeding ^{18}[F] to the synthesis module, the latter's vials are filled with different solutions: vial 1 with eluent reagent, vial 2 with 800 μl of DMSO containing 4 mg of 1-[*N*-(tert-butyloxy)carbamoyl]-3-(tosyl)ethyl-adamantane, vial 3 with 860 μl of 6 N hydrochloric acid solution, vial 4 with a mixture of 960 μl of 6 N caustic NaOH solution and 1 ml of 0.5 M trisodium citrate solution, vial 5 with 5 ml of acetonitrile, and vial 6 with 10 ml of water.

^{18}[F] is obtained through the nuclear reaction ^{18}O (p, n) ^{18}F by irradiation of a 95% ^{18}O-enriched water target (2.1 ml) with a 10 MeV proton beam in an IBA 10/5 cyclotron. After feeding ^{18}[F] from the cyclotron, the radioactivity is collected in a QMA Sep-Pak cartridge, where ^{18}[F] is trapped and $H_2^{18}O$ collected for recycling. A total of

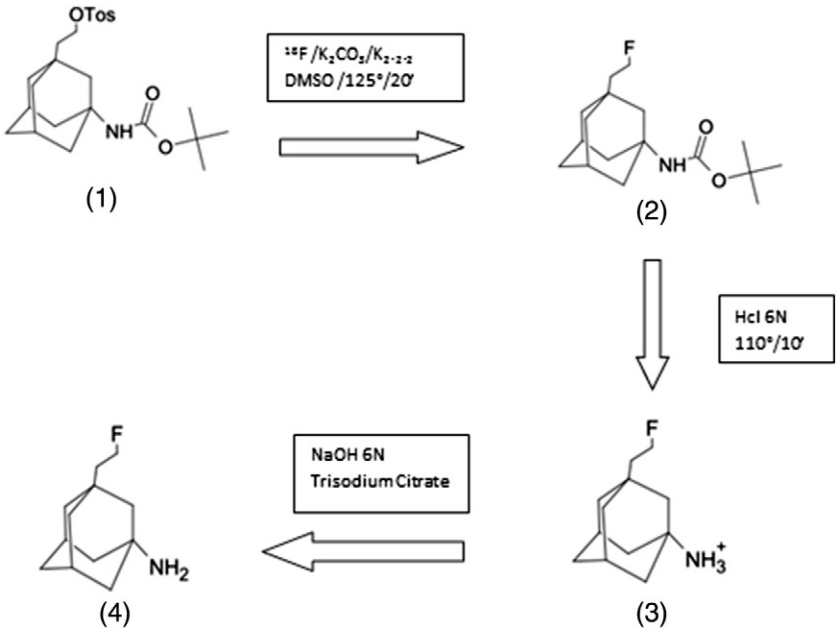

Fig. 1. Automatic synthesis of [^{18}F]-FNM in radiochemistry module. The first reaction corresponded to the nucleophilic substitution by fluorination of 1-[*N*-(tert-butyloxy)carbamoyl]-3-(tosyl)ethyl-adamantane (1) in DMSO. The fluorine compound (2) was hydrolyzed by hydrochloric acid at a high temperature (3) and subsequently neutralized to obtain 3-(2-fluoroethyl)tricyclo[3.3.1.13,7]decan-1-amine ([^{18}F]-FNM) (4).

600 μl of eluent-reagent solution is passed through the QMA Sep-Pak cartridge, from which the trapped [^{18}F] is sent to the reaction vessel. The solvent is evaporated under helium blanketing at 115 °C. After complete removal of the solvent by azeotropic drying, the precursor (1) is added to the reaction vessel and heated for 20 minutes at 125 °C. The reaction mixture is then cooled and added to the hydrolysis solution. The vessel is heated for 10 minutes at 110 °C, allowing for hydrolysis of the BOC (tert-butoxycarbonyle) groups. The reaction mixture is then cooled and neutralized by adding 6 N NaOH and 0.5 M trisodium citrate solutions.

Pre-purification is achieved using a Sep-Pak cartridge: the reaction mixture is trapped in a C_{18} Sep-Pak Plus and washed by 10 ml of water which pull free fluorine along. The lipophilic compound trapped in the cartridge is then eluted by 2 ml of absolute ethanol. The eluate passes through a liquid detector that controls the autosampler injector. HPLC purification is carried out in a semipreparative column (Cluzeau Info Labo Stability Basic CIL; 250 × 10 mm, particle size 5 μm), and the mobile phase is a 1 M ethanol/sodium acetate mixture (45/55). The [^{18}F]-FNM retention time is 15 minutes, with a flow rate of 2 ml/minute. The fraction of interest is collected and transferred to a distribution hot cell. The radioactivity and the volume of the product are then measured. The mother solution contains [^{18}F]-FNM: 3-(2-fluoroethyl)tricyclo[3.3.1.1^{3,7}]decan-1-amine. At the end of synthesis (T_0), volumic activity is measured. For animal experimentation, this mother solution is diluted in sodium chloride (0.9%) to obtain volumic activity of 200 MBq/ml.

2.1.3. Quality control and stability

Quality control of the final product was performed on a 4.6 × 150 mm Phenomenex Luna® analytic HPLC column coupled with two detectors: detector 1 measured radioactivity (NaI crystal), and detector 2 the UV signal (at 217 nm). Co-injection of the final product and the [^{19}F]-FNM reference allowed us to demonstrate that the synthesized compound corresponded to [^{18}F]-FNM. The mobile phase was a mixture of ethanol and sodium acetate (20/80). The same experiment was repeated at T_0 + 4 hours and T_0 + 6 hours to check the in vitro stability of the radio labeling. Acquisition was performed with AQUIS® (ICS software).

2.1.4. Log D determination

7.4 MBq of [^{18}F]-FNM was diluted in 10 ml phosphate buffer (pH = 7.4). Four aliquots from this sample (1 ml) were dispatched into four separate glass tubes. These tubes were spiked with 1 ml 1-octanol, vortexed for 5 minutes, and then centrifuged at 5 g for 5 minutes. The layers were then separated (top, organic; bottom, aqueous) and put into separate glass tubes. All the tubes were analyzed using a Wizard gamma counter.

2.2. Radioligand binding assay

The pharmacological binding assay of FNM was performed at Cerep (Poitiers, France). www.cerep.fr. Membrane homogenates were prepared according to this protocol: the rat brains without cerebella were rapidly removed and homogenized at 0 °C in 30 volumes of a 50 mM Tris-HCl buffer, pH 7.7, with a Brinkmann Polytron (setting 6) for 20 seconds. The homogenate was centrifuged at 49,000 × *g* for 15 minutes (corresponding to P2 fraction) and the resulting pellet was suspended in 30 volumes of the same Tris buffer. The homogenization and centrifugation steps were carried out twice. The final pellet was suspended in a 5 or 50 mM Tris-HCl buffer at pH 7.7 and used for binding experiments without further purification. We did not perform saturation binding experiment to obtain the Kd value of TCP, we used data as described in Vignon et al. [29].

Membrane homogenates of rat brain (140 μg of proteins) were incubated for 120 minutes at 37 °C with 10 nM [^{3}H]TCP(N-(1-[2-thienyl]-cyclohexyl)-3,4-piperidine) in the presence of an increasing dose of [^{19}F]-FNM (1.10^{-9} M to $1–10^{-5}$ M), in a buffer containing 5 mM Hepes/Tris (pH 7.4) and 0.1 mM EGTA. Nonspecific binding was determined in the presence of 10 μM (+) MK-801. After incubation, the samples were rapidly vacuum-filtered through glass fiber filters (GF/B, Packard) pre-soaked with 0.3% PEI and rinsed three times with ice-cold 50 mM Tris-HCl using a 96-sample cell harvester (Unifilter, Packard). The filters were dried, then counted for radioactivity in a scintillation counter (TopCount, Packard®) using a scintillation cocktail (Microscint 0, Packard). The standard reference compound is (+) MK 801 [30], which was tested in each experiment at several concentrations to obtain a competition curve from which the IC50 (inhibitory concentration) value was calculated. The IC 50 value for MK801 is 5.10^{-9} M. In parallel, a binding assay was performed with memantine (1.10^{-9} M to $1–10^{-5}$ M) and results were in agreement: IC 50 value was 1.10^{-6} M. This experiment was performed once. Kd used for TCP was 13 nM.

2.3. Animal experimentation

The goal of the project was to evaluate the biodistribution of [^{18}F]-FNM in rat brain. The first phase consisted in analyzing the brain pharmacokinetics of [^{18}F]-FNM. Two types of experiment were carried out: radioactivity well counting of different organs after autopsy of animals injected with [^{18}F]-FNM and PET imaging analysis. The purpose of these measurements was to define the length of time after injection needed to achieve the best signal on noise ratio, and define the sacrifice time to second phase. In the second phase (brain biodistribution analysis), we carried out both an in vitro investigation (immunohistochemistry with anti-NMDAr antibodies) and an ex vivo autoradiograph with [^{18}F]-FNM, in order to compare the respective distributions of NMDA receptors and NMDA-PCP sites in rat brain structures. In order to perform this comparison, the sections used for the immunochemistry were adjacent to those used for the autoradiography. Male Sprague–Dawley rats were used in all these experiments, weighing 350 ± 10 g. This protocol (no. 2014-26) was approved by Ethics Committee CEEA122 in France.

2.3.1. Pharmacokinetics

2.3.1.1. PET dynamic acquisition. One rat (360 g) anesthetized with 70 mg/kg of thiopental was injected with 85.92 MBq of [^{18}F]-FNM. Acquisition under the PET camera/CT began during injection of [^{18} F]-FNM and lasted 70 minutes (image size 256*300, 2-mm FWHM Gaussian filter, 6 iterations, 16 subsets). Images were analyzed using CARIMAS® software (http://www.turkupetcentre.fi/carimas/) to determine the time–activity curve in rat body. We chose several regions of interest (ROI) and manually traced the volume of interest (VOIs) on merged 3D PET-CT images. We selected seven VOIs in the brain cortex, cerebellum, heart, lung, spleen, kidney and liver.

2.3.1.2. Ex vivo biodistribution investigation. After intravenous administration of [^{18}F]-FNM: 8.7 MBq (0.024 nmoles), three rats per time point were killed by a lethal dose of pentobarbital at 30 or 60 minutes post injection. Each syringe was counted and weighed. Brains were washed in 0.9% saline solution and dissected. The following brain regions were isolated: cortex, cerebellum, ganglia and brain stem. These four regions, as well as blood (obtained just before euthanasia), were counted in a well counter for [^{18}F] and weighed. A reference sample of the injected dose was also weighed and counted, to evaluate the proportion of the injected dose that remained in each region and tissue (to avoid having to correct for radioactive decay). We also corrected this count with the residual activity in the injection syringe.

2.3.2. Immunohistochemistry and ex vivo autoradiography

We performed these experiments with four male rats that had been anesthetized with isoflurane. [^{18}F]-FNM was injected via a catheter introduced into the tail vein. Injected doses of [^{18}F]-FNM were 92.7 ± 7 MBq (0.26 nmoles). Doses were higher than those previously evaluated, as radioactivity was measured in 20 μm thick sections of brain, and sufficient activity was required to be able to measure activity 40 minutes after injection of the radiotracer. Rats were euthanized by intravenous injection of pentobarbital (100 mg/kg). After exsanguination, their brains were removed and then frozen in isopentane cooled to −50 °C with liquid nitrogen. The brains were then sectioned with a cryostat and 20 μm thick sagittal sections collected on slides. These sections were placed in contact with a phosphor screen overnight. This screen was then developed on a Typhoon® FLA 9400 phosphorimager (1 pixel = 25 μm). This step allowed us to test in vivo specificity and confirm crossing of the blood brain barrier.

Moreover we performed an experiment with a rat anesthetized with ketamine instead of isoflurane. Ketamine is an NMDA antagonist, binding to the same site as [^{18}F]-FNM. It was injected at a pharmacological dose (80 mg/kg) in order to saturate the PCP binding sites. This cross check allowed us to test the binding specificity of [^{18}F]-FNM.

Immunochemistry was performed on sections adjacent to those used for autoradiography. These sections were left to dry for 2 hours at room temperature, and prefixed with acetone for 10 minutes. Slides were stored at −20 °C until the histological analysis. They were then warmed at room temperature and postfixed with acetone for 10 minutes. No permeabilization was performed. They were washed three times (5 minutes) with phosphate buffer saline (PBS 50 mM, pH = 7.4) and incubated in PBS with 3% goat serum for 30 minutes.

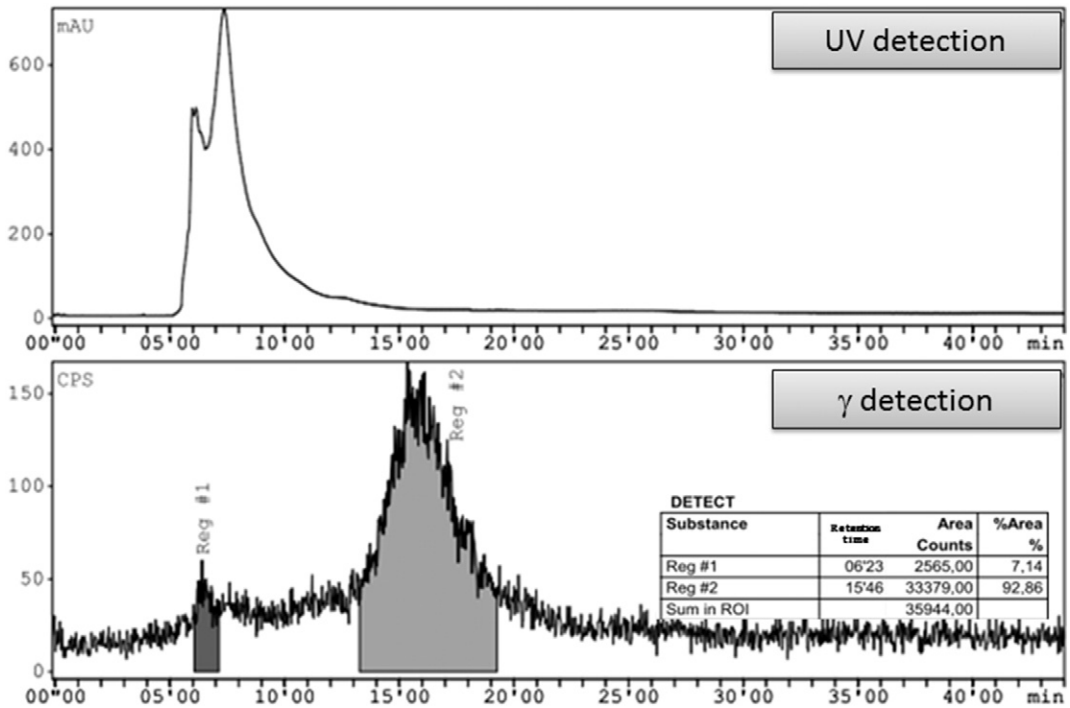

Fig. 2. Semipreparative purification diagram. UV detection showed that there were no chemical impurities in the [^{18}F]-FNM peak (represented by "Reg# 2" in gamma detection). Retention time of [^{18}F]-FNM in semipreparative purification was 15–16 minutes.

They were then incubated with the primary antibody 1:100 (Invitrogen™ Mouse anti-NMDA Receptor Subunit 1, IgG2a, clone 54.1), for 72 hours at 4 °C. After three baths of 5 minutes in PBS at room temperature, the slides were incubated with PBS containing secondary fluorescent antibody 1:1000 (Alexa Fluor® Anti-Mouse 488) for 2 hours, then washed again three times (5 minutes) with PBS. Incubation with DAPI was performed for 10 minutes to label cell bodies. Slides were washed three times and allowed to dry. Sections were then cover slipped with a fluorescent mounting medium (DAKO).

2.3.3. Data acquisition, data processing and statistical test

The exposed phosphor screen and the immunofluorescent brain sections were placed on the glass platen of the Typhoon® FLA 9400. They were illuminated with a red laser (633 nm) for the phosphor screen, and a green laser for the immunostained brain sections. The phosphorus emitted a blue light and the fluorochrome a light with a characteristic spectrum. The optical system collected the emitted light and the photomultiplier tube converted this light to an electric current, which varied proportionally to the intensity of the light collected. The analog signal was then converted into digital light units (DLUs). ImageQuant software mapped the digital information to the appropriate pixel location on the monitor and produced an accurate image of the original sample. We then processed the data (.gel images) obtained from immunostained and autoradiographied sections with ImageJ software. With plugin stitching of ImageJ software, images of two adjacent sections, one immunostained and one radiolabeled could be automatically merged. On each merged image, we then drew 7 ROIs cortex, white matter (corpus callosum), brain stem, olfactory bulb, thalamus, hippocampus and cerebellum. On average, the selected areas measured 0.0021 cm^2. We have chosen sagittal section to have many cerebral structure in the same sample (especially cerebellum), and to be able to compare uptake intensity in the same section. Each section contained all seven ROIs.

Measurements were made on six pairs of brain sections obtained from two rats ($n = 2$) (three pairs from rat 1 and three pairs from rat 2), chosen at similar level in the brain. Pairs comprising adjacent sections (one IHC; one autoradiography) and automatized matched images (ImageJ stitching plugin) were not always achievable, owing to cryostat section cutting variability. For the colocalization analysis in the ketamine anesthetized rat, we used two pairs of brain sections.

We chose the ROI on the basis of Petralia et al.'s description of the distribution of NMDA Receptor Subunit NR1 in the rat nervous system [31]. ROIs were drawn on the merged image, allowing us to obtain a signal in the same area from the channel measuring immunolabeling and a signal from the channel measuring autoradiography.

For the analysis of autoradiography data, differences in the regions' intensity values were tested with an analysis of variance (ANOVA) and Student's *t* test. As the data for the colocalization analysis (7 ROIs on 6 paired sections = 42 values for the isopentane anesthetized rats, and 7 ROIs on 2 paired sections = 14 values for the ketamine anesthesia condition were non-normally distributed (Kolmogorov–Smirnov test), we used the Spearman rank correlation coefficient (Xcel stat software).

3. Results and discussion

3.1. Radiochemical synthesis

3.1.1. HPLC purification and balance yield

HPLC purification of crude products showed only two radioactive peaks (Fig. 2): the first peak was a match for free fluoride, and the second, measured at 15 minutes, corresponded to [^{18}F]-FNM. No other radioactive impurities appeared on the chromatogram, as they were eliminated during the pre-purification phase. [^{18}F]-FNM eluted from the Sep-Pak cartridge was separated from the unreacted material and radioactive impurities by means of isocratic reverse-phase HPLC. We can therefore assume that the first prepurification was not sufficient, as we still found 10.6 ± 3.05% of free fluorine on the semipreparative purification diagram.

Five syntheses were successfully performed. The radiochemical yield was 10.5% ± 3%, with average activity of [^{18}F]-FNM at 3145 MBq. Specific activity of [^{18}F]-FNM was above 355 GBq/μmol.

3.1.2. Quality control and stability

[^{18}F]-FNM was eluted with a mixture of ethanol and sodium acetate (20/80). Flow rate was 1.5 ml/minute, and retention time was 9.8 minutes. At end of synthesis, 100% of radiochemical purity was observed. The same analytical HPLC was performed 4 and 6 hours after the end of synthesis, and we observed no significant difference in radiochemical purity. On the UV diagram, a small peak of impurity was detected at 4 minutes. This impurity was not characterized. (Fig. 3)

3.1.3. Log D determination

Determination of log D was performed on four samples of 1 ml, each containing 740 kBq, in the condition mentioned in the Method section. The log D of [^{18}F]-FNM was 1.93.

3.2. Radioligand binding assay

This competition experiment allowed us to determine that the IC 50 value FNM is equal to 6.1 10^{-6} M and the Ki value was 3.5 μM.

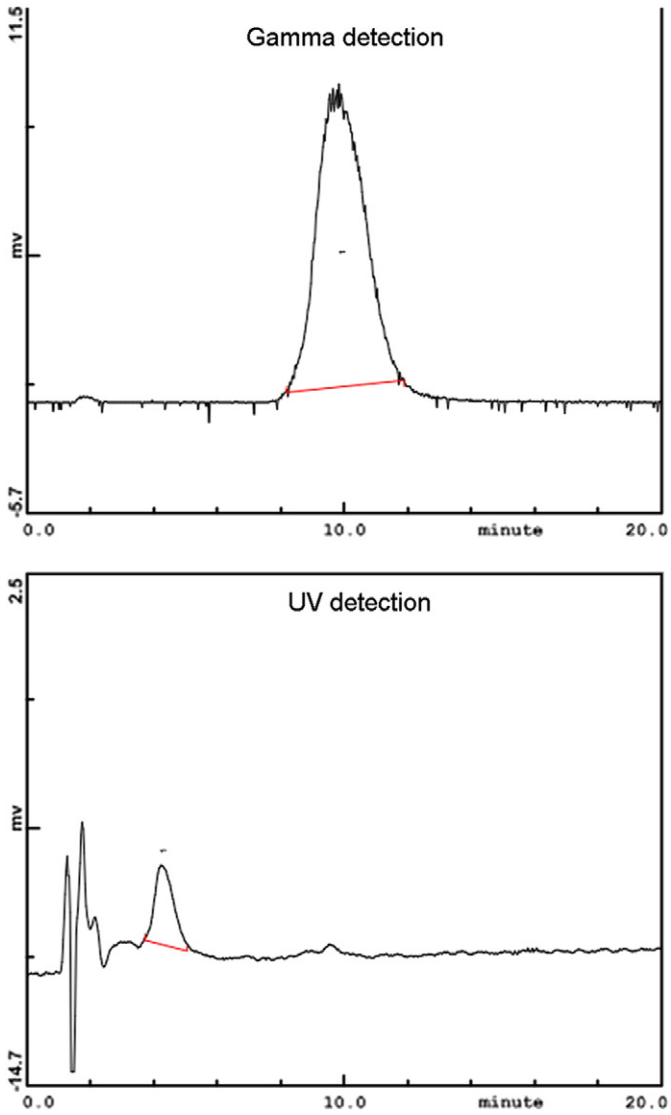

Fig. 3. Analytic purification diagram. UV detection showed a little peak at 4 minutes corresponding to an unknown impurity. Radiochemical purity is 99%.

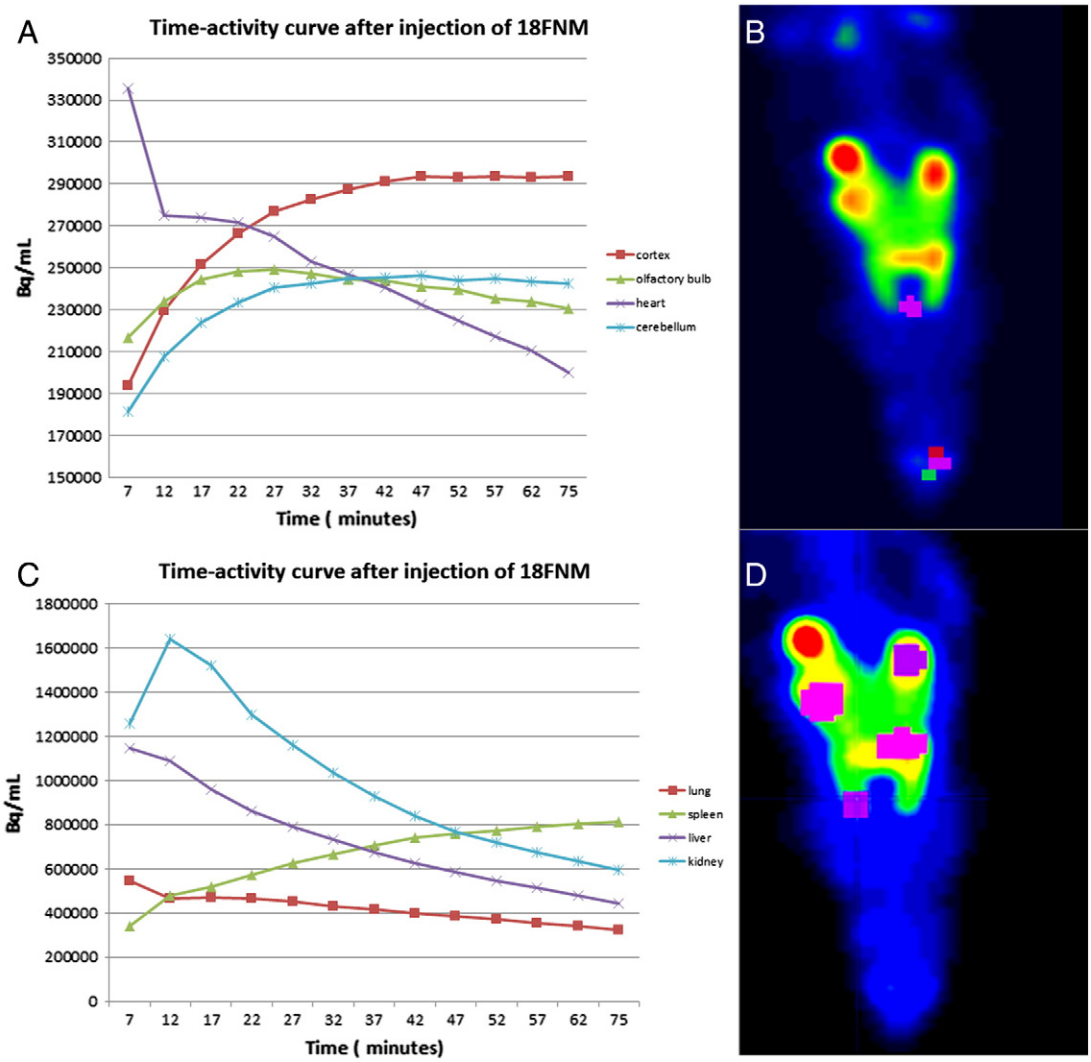

Fig. 4. Time–activity curve based on VOI analysis on Carimas software after injection of 119 MBq of [^{18}F]-FNM. A: Time activity/curve in the brain C: Time activity curve in whole body. B and D represent PET uptake profile in rat (head at the bottom) and regions of interest.

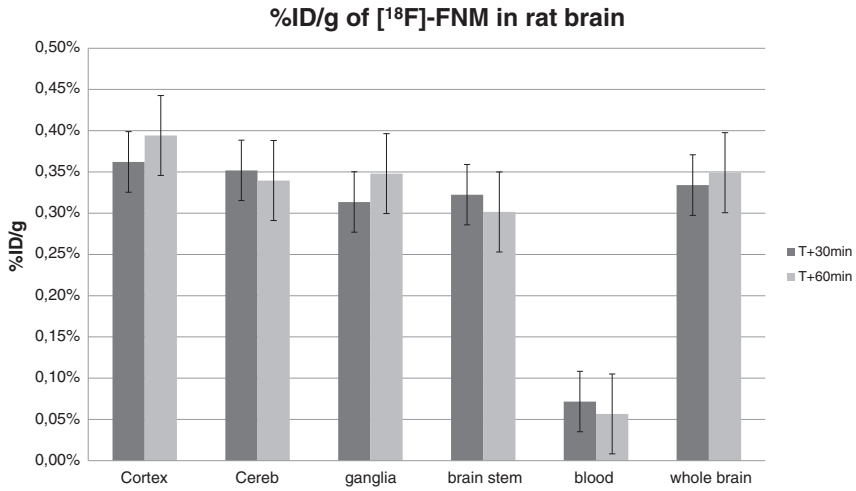

Fig. 5. Percentage of the injected dose (ID/g of tissue) in different rat brain regions and in the blood. Values observed 30 minutes (T + 30 minutes) and 1 hour (T + 60 minutes) after injection of [^{18}F]-FNM.

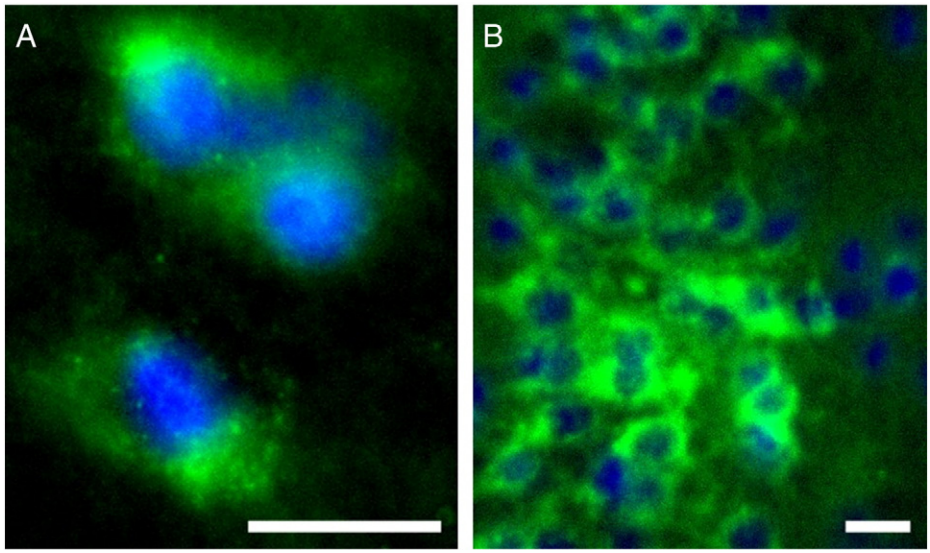

Fig. 6. NMDAR1 immunostaining in the rat hippocampus region. Very dense staining was seen in the pyramidal neurons of CA-1 and CA-3 in hippocampus. Scale bar 50 μm.

Memantine, used as a reference compound to evaluate the applied versus published assay, presents an IC 50 value of 1.1 10^{-6} M. This value is in agreement with the data published in the literature [32].

3.3. Animal experimentation

3.3.1. Pharmacokinetics

3.3.1.1. PET dynamic acquisition. The time–brain activity curve showed that brain uptake of [^{18}F]-FNM in the rat gradually increased across the first 40 minutes, as shown in Fig. 4A. During this period we observed a decrease in the vascular signal (heart). A good signal-on-noise ratio was obtained after 40 mn post injection. These results explain why we chose to sacrifice rats for autoradiography at 40 minutes post injection. Kidney elimination was a significant clearance pathway, resulting in a maximum tracer concentration of 1.12% injected dose per gram (ID/g) in the kidneys at 7 minutes, decreasing to 0.57% ID/g at 62 minutes. We found little accumulation in the spleen, or uptake in the liver and lung (Fig. 4C). There was no accumulation in bone (data not shown), suggesting that there is no in vivo defluorination of this compound.

3.3.1.2. In vivo rat biodistribution studies. The brain-to-blood ratio increased from 4.74 to 6.19 between 30 and 60 minutes post injection. These values were not significantly different in the *t* test ($p = 0.08$), and the *p* value for the permutation method (30 permutations) was 0.067. At 60 minutes post injection, 0.34% of the ID/g was in the brain. The highest level of radioactivity was found in the cortex: 0.36% ID/g (Fig. 5). Mean % ID/g was higher at 60 minutes than at 30, so results confirmed the preliminary biodistribution analysis, suggesting that autoradiography should be performed 40 minutes post injection.

3.3.2. Immunohistochemistry and ex vivo autoradiography

3.3.2.1. Immunohistochemistry. With light microscopy, we observed the classic distribution of GluN1, as revealed in the rat brain tissue by immunostaining (Fig. 6) [31]. Macroscopically, the signal was intense in cortical regions, as well as in the hippocampus, thalamus and cerebellum, and low in white matter Fig. 7A. A similar pattern was seen in the rats anesthetized with isoflurane or ketamine.

3.3.2.2. Autoradiography. In the isoflurane-anesthetized rats, the signal was diffuse, but uptake was high in cortical regions, the cerebellum and the hippocampus. Uptakes were weaker and diffuse in white matter (Fig. 7B). In the ketamine-anesthetized rat, uptake was weak, diffuse and homogenous. No differences were macroscopically observed between the brain regions (not shown).

The autoradiography signal was measured in the seven ROIs: corpus callosum, cerebellum, brain stem, olfactory bulb, thalamus, hippocampus and cortex, in six sections. An ANOVA on these values showed an intergroup effect ($p = 8.5\ 10^{-15}$). Three uptake profiles were observed, with a significant difference in the post hoc *t* test ($p < 0.005$): low uptake in white matter, medium uptake in the brain stem, olfactory bulb, thalamus and hippocampus, and higher uptake in the cerebellum and cortex. No significant difference was found between the hippocampus, brain stem, thalamus and olfactory bulb (Fig. 8).

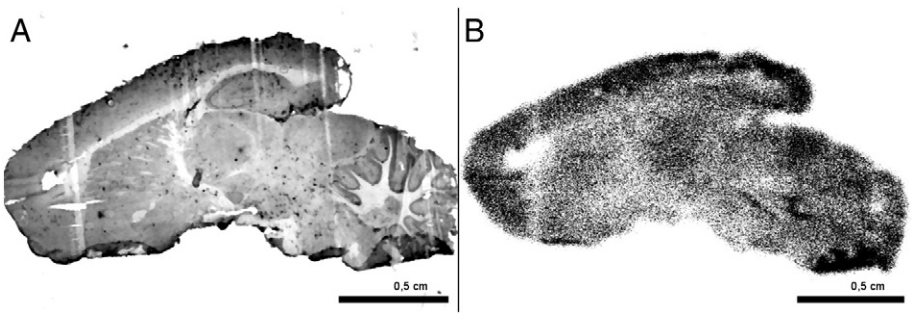

Fig. 7. Immunostaining (NMDAR1, A) and autoradiogaphy ([^{18}F]-FNM, B) of two adjacent brain sections (20 μm thick) from a rat anesthetized with isoflurane.

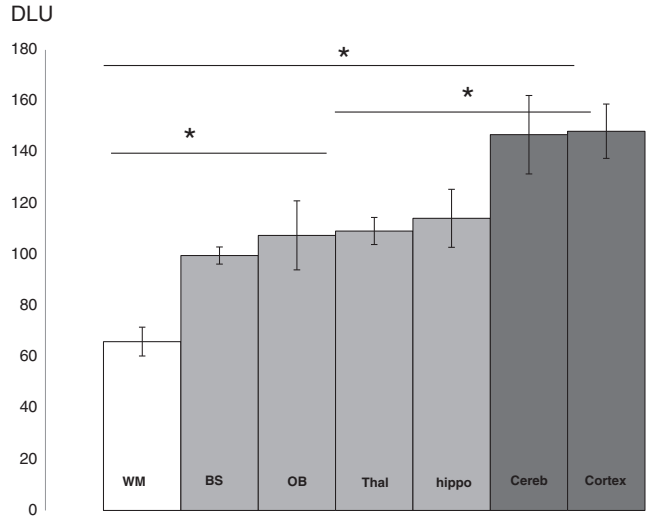

Fig. 8. Autoradiography analysis: mean intensity signal of 6 sections from 2 rats. Seven ROIs were drawn and analyzed in each section. WM: white matter (corpus callosum); BS: brain stem; OB: olfactory bulb; Thal: thalamus; Hippo: hippocampus; Cereb: cerebellum; DLU: digital light unit. *: $p < 0.005$.

3.3.2.3. Correlation analysis. Immunostaining intensity level was evaluated on the sections adjacent to the autoradiography sections. Signal intensities in radiolabelled, and immunostained sections were plotted. In the rats anesthetized with isoflurane (Fig. 9A), the autoradiography signal was significantly correlated with intensity of immunohistochemical staining ($R^2 =$ 0.85 reliability factor of the fitted curve). This result was confirmed by the result of the Spearman test on these 42 raw data was $r = 0.622$, $p < 0.0001$.

The same method was used for the ketamine-anesthetized rat. No correlation between autoradiography and immunostaining intensities was found ($R^2 = 0.027$; statistical control of noncorrelation with nonparametric test of permutation method: $p = 0.0002$, $R^2 \geq 0.027$). The result of the Spearman test was $r = -0.527$, $p = 0.067$ (Fig. 9B).

4. Discussion

4.1. Radiosynthesis

[^{18}F]-FNM was successfully synthesized using the Raytest® radiochemistry module. This was the first time that this memantine derivative had been synthesized. The fluorination yield was weak, but recorded activity was compatible with preclinical imaging. Enhancement of the synthesis process is currently underway. We used an acetate/ethanol mixture for HPLC purification which, after pharmaceutical formulation, gave a ready-to-use solution free from dangerous solvents such as acetonitrile or DMSO. Moreover this method saved time (no need to remove acetonitrile by evaporation), and resulted in a safer product for preclinical studies. A non-characterized impurity was detected in the UV analytical diagram. Although this impurity is in tiny quantity, its characterization should be achieved in order to safely use this radiotracer in clinical applications because this impurity could be pharmacologically active.

4.1.1. Properties of the new radioligand

Affinity of [^{18}F]-FNM (IC 50: 6.1 10^{-6} M), investigated by in vitro binding assay, was poor compared with ketamine or MK-801 (Ki = 79 nM) [12,33]. Nonetheless, [^{18}F]-FNM seems to bind less with white matter than other PET probes, and therefore yields a better signal-on-noise ratio. Autoradiography showed an obviously poor uptake by fiber tracts. The BBB crossing test showed that at 60 minutes after injection, 0.34% DI/g of [^{18}F]-FNM was in the brain, with the highest level of radioactivity in the cortex. This value is sufficient, but could be increased further by the synthesis of other memantine derivatives. Chemical modification can modulate specificity and BBB crossing, and we could work on several derivatives, although it is important to preserve affinity for the receptor. The first memantine derivative tested ([^{18}F]-FMEM) had better BBB crossing (3.6% ID/g [19]) and similar affinity, but was rejected because of excessive interindividual variation and surprising kinetic behavior in white matter, as quantified by a two-tissue compartment model. The present memantine derivative seems to have a lower uptake in white matter, and could be a useful compound to carry on investigating in the memantine family. Results of colocalization suggest that [^{18}F]-FNM binding is highly correlated with the physiological distribution of NMDA receptors in the rat brain. As shown in Fig. 9, the brain distribution of [^{18}F]-FNM closely matched that of NMDAr1. Assessment with ketamine (injected at a pharmacological dose) allows us to consider that detected [^{18}F]-FNM binding is specific, as no correlation was found between ex vivo autoradiography and immunostaining when this antagonist was injected before [^{18}F]-FNM. However, the specificity of the binding as specified below is still to prove because of the effect of ketamine in pharmacological dose.

4.1.2. Limitation

We compare here only autoradiography results and immunostaining but we cannot compare result of the two autoradiography intensity

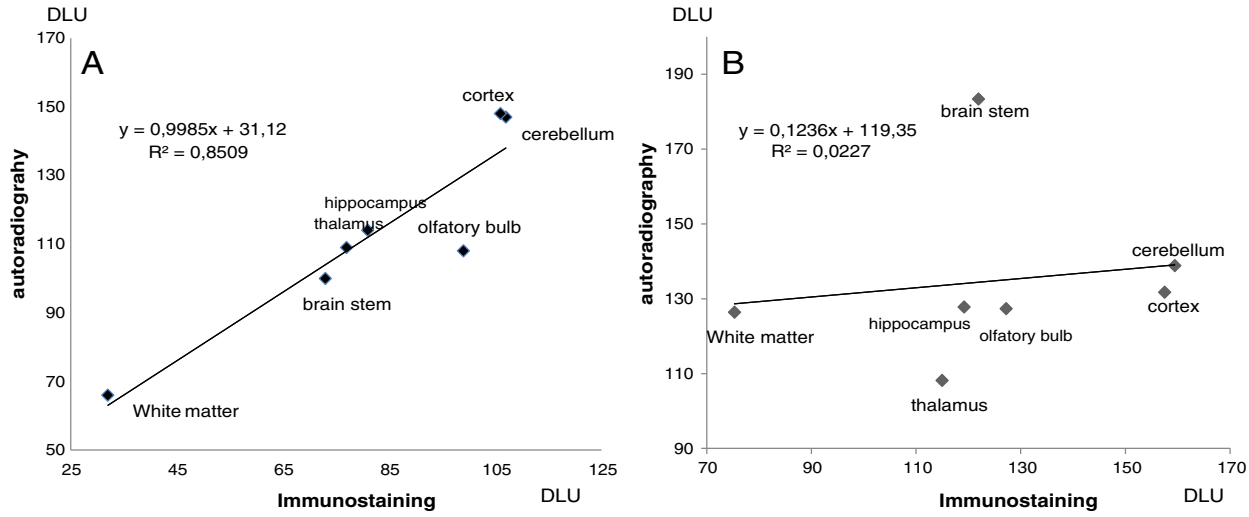

Fig. 9. Correlation analysis between autoradiography and immunostaining. Analysis in seven different brain regions. A: rats (2) anesthetized with isoflurane, B: rat anesthetized with ketamine.

results (isoflurane and ketamine) together. Although, [^{18}F]-FNM binding in the control rat (competition assay) appeared to be very different from that of the rats anesthetized with isoflurane, uptake comparison between the two experiments is not possible. Many anesthetic drugs distort cerebral blood flow, cerebral concentration on amino acid or primary depolarization that is necessary to have an open state of NMDAr. Rozza et al. have shown that anesthesia induced by ketamine caused a significant decrease in the levels of glutamate, aspartate and glycine. Therefore, as we used two different anesthetic drugs (ketamine or isoflurane), we have a different impact of these phenomena and that can cause difference between uptake and washout kinetic [34,35]. There is also another limitation for the quantification of radioactivity in the brain; euthanasia was performed with overdose of anesthetic, so other studies using decapitation could allow us to compare disturbance caused by the overdose method.

4.1.3. Future

The present study was conducted with normal rats, in a classical condition. No pathological situation has yet been investigated with [^{18}F]-FNM. Now that we have shown that the radiotracer specifically binds to the open NMDAr, experiments can be planned to examine whether it can be used to detect pathological conditions. It has been demonstrated that dynamic changes take place in NMDA-receptors after closed head injury in mice [36]. Using a [^{3}H]PCP antagonist, Biegon et al. demonstrated a shift from the closed to the open state of the NMDAr. They thus described hyperactivation for a very short period (15 minutes) after injury, followed by hypoactivation lasting 8 hours. A specific lesion with an NMDA activator in the hippocampus or cortex could provide a good opportunity to test whether [^{18}F]-FNM is able to locate affected areas and reveal the dynamics of hyperactivity.

5. Conclusion

Given the constant interest in NMDA receptors for neuropsychopharmacology, and the current lack of fluorinated PET radiotracers, the present study paves the way to identifying more specific ligands of NMDA receptors. [^{18}F]-FNM seems to be a promising basis for designing suitable compounds for imaging NMDA activation and for undertaking the clinical detection of neurological or neuropsychological disorders.

Competing interests

The authors declare that they have no competing interests.

Authors' contributions

ASS was involved in the design of the study, data collection, and initial writing of the manuscript. ASS, CaF, CP, ChF and MA carried out the animal autopsies and checked the manuscript. ASS, MA and MT carried out tracer synthesis. ASS, PP, MT, HB contributed to the conception of the study. DA helped with the statistical analysis. All the authors read and approved the final manuscript.

Abbreviations

BBB	blood–brain barrier
BOC	tert-butoxycarbonyle
DLU	digital light unit
DMSO	dimethylsulfoxyde
[^{18}F]-FNM	fluoroethylnormemantine
MBq	mega becquerel
HPLC	high performance liquid chromotography
IC	inhibitory concentration
ID/g	injected dose per gram
Kd	dissociation constant; Ki inhibition constant
NMDAr	*N*-methyl-D-aspartate receptor
PCP	phencyclidine
ROI	region of interest
TCP	*N*-(1-[2-thienyl]-cyclohexyl)-3,4-piperidine

Acknowledgments

The authors acknowledge the support of M2I development for developing and supplying the [^{18}F]-FNM precursor and the [^{19}F]-FNM reference.

We are grateful to the staff of the animal experimentation platform of joint research unit UMS 006 for their advice, and to the staff of the Genotoul proteomic platform for their technical assistance.

This work has been supported in part by a grant from the French National Agency for Research, called “Investissements d’Avenir”.

References

[1] Sahai S. Glutamate in the mammalian CNS. Eur Arch Psychiatry Clin Neurosci 1990; 240:121–33.
[2] Dingledine R, Borges K, Bowie D, Traynelis SF. The glutamate receptor ion channels. Pharmacol Rev 1999;51:7–61.
[3] Chen H-SV, Lipton SA. The chemical biology of clinically tolerated NMDA receptor antagonists. J Neurochem 2006;97:1611–26.
[4] Villmann C, Strutz N, Morth T, Hollmann M. Investigation by ion channel domain transplantation of rat glutamate receptor subunits, orphan receptors and a putative NMDA receptor subunit. Eur J Neurosci 1999;11:1765–78.
[5] Paarmann I, Frermann D, Keller BU, Villmann C, Breitinger HG, Hollmann M. Kinetics and subunit composition of NMDA receptors in respiratory-related neurons. J Neurochem 2005;93:812–24.
[6] Tao-Cheng J-H. Ultrastructural localization of active zone and synaptic vesicle proteins in a preassembled multi-vesicle transport aggregate. Neuroscience 2007;150: 575–84.
[7] Petralia RS. Distribution of extrasynaptic NMDA receptors on neurons. Sci World J 2012;2012:1–11.
[8] Bordji K, Becerril-Ortega J, Nicole O, Buisson A. Activation of extrasynaptic, but not synaptic, NMDA receptors modifies amyloid precursor protein expression pattern and increases amyloid-production. J Neurosci 2010;30:15927–42.
[9] Hu N-W, Ondrejcak T, Rowan MJ. Glutamate receptors in preclinical research on Alzheimer's disease: update on recent advances. Pharmacol Biochem Behav 2012; 100:855–62.
[10] Gee CE, Benquet P, Raineteau O, Rietschin L, Kirbach SW, Gerber U. NMDA receptors and the differential ischemic vulnerability of hippocampal neurons. Eur J Neurosci 2006;23:2595–603.
[11] Sobrio F. Radiosynthesis of carbon-11 and fluorine-18 labelled radiotracers to image the ionotropic and metabotropic glutamate receptors. J Label Compd Radiopharm 2013;56:180–6.
[12] Waterhouse RN. Imaging the PCP site of the NMDA ion channel. Nucl Med Biol 2003; 30:869–78.
[13] Majo VJ, Prabhakaran J, Mann JJ, Kumar JSD. PET and SPECT tracers for glutamate receptors. Drug Discov Today 2013;18:173–84.
[14] Blin J, Denis A, Yamaguchi T, Crouzel C, MacKenzie ET, Baron JC. PET studies of [18 F]methyl-MK-801, a potential NMDA receptor complex radioligand. Neurosci Lett 1991;121:183–6.
[15] Shiue CY, Vallabhahosula S, Wolf AP, Dewey SL, Fowler JS, Schlyer DJ, et al. Carbon-11 labelled ketamine-synthesis, distribution in mice and PET studies in baboons. Nucl Med Biol 1997;24:145–50.
[16] Orita K, Sasaki S, Maeda M, Hashimoto A, Nishikawa T, Yugami T, et al. Synthesis and evaluation of 1-(1-[5-(2′-[18 F]fluoroethyl)-2-thienyl]-cyclohexyl)piperidine as a potential in vivo radioligand for the NMDA receptor-channel complex. Nucl Med Biol 1993;20:865–73.
[17] Ametamey SM, Bruehlmeier M, Kneifel S, Kokic M, Honer M, Arigoni M, et al. PET studies of 18 F-memantine in healthy volunteers. Nucl Med Biol 2002;29:227–31.
[18] Ametamey SM, Samnick S, Leenders KL, Vontobel P, Quack G, Parsons CG, et al. Fluorine-18 radiolabelling, biodistribution studies and preliminary PET evaluation of a new memantine derivative for imaging the NMDA receptor. J Recept Signal Transduct Res 1999;19:129–41.
[19] Samnick S, Ametamey S, Leenders KL, Vontobel P, Quack G, Parsons CG, et al. Electrophysiological study, biodistribution in mice, and preliminary PET evaluation in a rhesus monkey of 1-amino-3-[18 F]fluoromethyl-5-methyl-adamantane (18 F-MEM): a potential radioligand for mapping the NMDA-receptor complex. Nucl Med Biol 1998;25:323–30.
[20] Sasaki S, Kanda T, Ishibashi N, Yamamoto F, Haradahira T, Okauchi T, et al. 4,5,9,10-Tetrahydro-1,4-ethanobenz[b]quinolizine as a prodrug for its quinolizinium cation as a ligand to the open state of the TCP-binding site of NMDA receptors. Bioorg Med Chem Lett 2001;11:519–21.

[21] Sasaki S, Ishibashi N, Kuwamura T, Sano H, Matoba M, Nisikawa T, et al. Excellent acceleration of the Diels-Alder reaction by microwave irradiation for the synthesis of new fluorine-substituted ligands of NMDA receptor. Bioorg Med Chem Lett 1998; 8:2983–6.
[22] Robins EG, Zhao Y, Khan I, Wilson A, Luthra SK, Årstad E. Synthesis and in vitro evaluation of 18 F-labelled S-fluoroalkyl diarylguanidines: Novel high-affinity NMDA receptor antagonists for imaging with PET. Bioorg Med Chem Lett 2010; 20:1749–51.
[23] McGinnity CJ, Hammers A, Riano Barros DA, Luthra SK, Jones PA, Trigg W, et al. Initial evaluation of 18 F-GE-179, a putative PET tracer for activated *N*-methyl D-aspartate receptors. J Nucl Med 2014;55:423–30.
[24] Golla SSV, Klein PJ, Bakker J, Schuit RC, Christiaans JAM, van Geest L, Kooijman EJM, Oropeza-Seguias GM, Langermans JAM, Leysen JE, Boellaard R, Windhorst AD, van Berckel BNM. Metaxas A: Preclinical evaluation of [18 F]PK-209, a new PET ligand for imaging the ion-channel site of NMDA receptors. Nucl Med Biol; 2014.
[25] Hardingham GE, Bading H. Synaptic versus extrasynaptic NMDA receptor signalling: implications for neurodegenerative disorders. Nat Rev Neurosci 2010;11: 682–96.
[26] Xia P, Chen H-sV, Zhang D, Lipton SA. Memantine preferentially blocks extrasynaptic over synaptic NMDA receptor currents in hippocampal autapses. J Neurosci 2010; 30:11246–50.
[27] Wu Y-N, Johnson SW. Memantine selectively blocks extrasynaptic NMDA receptors in rat substantia nigra dopamine neurons. Brain Res 2015;1603:1–7.
[28] Wild AR, Akyol E, Brothwell SLC, Kimkool P, Skepper JN, Gibb AJ, et al. Memantine block depends on agonist presentation at the NMDA receptor in substantia nigra pars compacta dopamine neurones. Neuropharmacology 2013;73:138–46.
[29] Vignon J, Privat A, Chaudieu I, Thierry A, Kamenka JM, Chicheportiche R. [3H]thienylphencyclidine ([3H]TCP) binds to two different sites in rat brain. Localization by autoradiographic and biochemical techniques. Brain Res 1986;378:133–41.
[30] Bresink I, Danysz W, Parsons CG, Mutschler E. Different binding affinities of NMDA receptor channel blockers in various brain regions—indication of NMDA receptor heterogeneity. Neuropharmacology 1995;34:533–40.
[31] Petralia RS, Yokotani N, Wenthold RJ. Light and electron microscope distribution of the NMDA receptor subunit NMDAR1 in the rat nervous system using a selective anti-peptide antibody. J Neurosci Off J Soc Neurosci 1994;14:667–96.
[32] Kornhuber J, Bormann J, Hübers M, Rusche K, Riederer P. Effects of the 1-aminoadamantanes at the MK-801-binding site of the NMDA-receptor-gated ion channel: a human postmortem brain study. Eur J Pharmacol 1991;206:297–300.
[33] Labas R, Gilbert G, Nicole O, Dhilly M, Abbas A, Tirel O, et al. Synthesis, evaluation and metabolic studies of radiotracers containing a 4-(4-[18 F]-fluorobenzyl)piperidin-1-yl moiety for the PET imaging of NR2B NMDA receptors. Eur J Med Chem 2011;46: 2295–309.
[34] Rozza A, Masoero E, Favalli L, Lanza E, Govoni S, Rizzo V, et al. Influence of different anaesthetics on extracellular aminoacids in rat brain. J Neurosci Methods 2000;101: 165–9.
[35] Martin DC, Plagenhoef M, Abraham J, Dennison RL, Aronstam RS. Volatile anesthetics and glutamate activation of *N*-methyl-D-aspartate receptors. Biochem Pharmacol 1995;49:809–17.
[36] Biegon A, Fry PA, Paden CM, Alexandrovich A, Tsenter J, Shohami E. Dynamic changes in *N*-methyl-D-aspartate receptors after closed head injury in mice: implications for treatment of neurological and cognitive deficits. Proc Natl Acad Sci U S A 2004;101: 5117–22.